KEK Preprint 2003-2
April 2003
H

Low-Energy Photon Collider

R. BELUSEVIC

High Energy Accelerator Research Organization

High Energy Accelerator Research Organization (KEK)

KEK Reports are available from:

Information Resources Division
High Energy Accelerator Research Organization (KEK)
1-1 Oho, Tsukuba-shi
Ibaraki-ken, 305-0801
JAPAN

Phone: +81-29-864-5137
Fax: +81-29-864-4604
E-mail: irdpub@mail.kek.jp
Internet: http://www.kek.jp

"*The changing of bodies into light, and light into bodies, is very conformable to the course of nature, which seems delighted with transmutations.*"

Isaac Newton

1 Raisons d'être for a photon collider

The aim of this note is to propose the construction of a (110 to 200)-GeV photon collider at KEK. This unique machine would take us beyond the LEP era, and thus bridge the gap between the present HEP frontier and that to be reached by a future e^+e^- collider. The physics at such a facility would be complementary to that at an electron-positron linac.

The set of final states at a photon collider is richer than that in e^+e^- collisions. Since photons couple directly to all fundamental fields carrying the electromagnetic current (leptons, quarks, W bosons, supersymmetric particles), $\gamma\gamma$ collisions provide a comprehensive means of exploring virtually every aspect of the Standard Model and its extensions. The production mechanisms in e^+e^- collisions are often more complex and model-dependent.

The cross-sections for production of charged particle pairs in a $\gamma\gamma$ collision are 5 to 8 times larger than those in an e^+e^- annihilation (for WW production, this factor is about 10 to 20), and many of them increase with energy. In contrast, the corresponding e^+e^- cross-sections scale as $1/s$.

In $\gamma\gamma$ collisions the Higgs boson will be produced as a single resonance in a state of definite CP, which is perhaps the most important advantage over e^+e^- annihilations, where this s-channel process is highly suppressed. For the Higgs mass in the range (120 to 250) GeV, the effective cross-section for $\gamma\gamma \to h$ is 6 to 30 times larger than that for the Higgs production in e^+e^- annihilations.

Since $\gamma\gamma \to h$ proceeds through a 'loop diagram' and receives contributions from *all* particles with mass and charge, this mode is a powerful probe of new physics beyond the Standard Model.

2 Compton scattering

The idea of photon colliders was first put forward in 1981 by the Russian physicists Ilya Ginzburg, Gleb Kotkin, Valery Serbo and Valery Telnov. Their seminal paper on the subject describes in detail a method of obtaining photon-photon ($\gamma\gamma$) and electron-photon ($e\gamma$) colliding beams by Compton backscattering of laser light on high-energy electrons [1]. The backscattered photons have energies comparable to those of the incident electrons, and follow their direction with some small angular spread of the order of $1/\gamma$, where $\gamma = \mathrm{E}/m_e c^2$ is the Lorentz factor. The spatial spread of the photons is approximately d/γ at a distance d from the Compton interaction point. If the laser beam is sufficiently intense,. the luminosity of $\gamma\gamma$ and $e\gamma$ collisions can be of the same order of magnitude as the 'geometric' luminosity of the incident ee beams. [1]

[1] The *geometric luminosity*, $\mathcal{L}_{ee}$, is defined as the interaction rate per unit cross-section: Rate $= \mathcal{L}_{ee}\,\sigma$. If n is the number of particles in a 'bunch', b the number of bunches per pulse, f the pulse repetition frequency and A the transverse area of the beam, then the event rate is

$$\text{Rate} = (n^2 bf/A)\,\sigma = \mathcal{L}_{ee}\,\sigma$$

For a Gussian density distribution with transverse rms radii σ_x and σ_y, $A = 4\pi\sigma_x\sigma_y$. Introducing the beam current $\mathcal{I} = n\,\mathrm{e}\,bf$, where e is is the magnitude of the electron charge, we have

$$\mathcal{L}_{ee} = \frac{\mathcal{I}^2}{4\pi\mathrm{e}^2}\,\frac{(bf)^{-1}}{\sigma_x\sigma_y}$$

It should be noted that, due to beam-beam effects, $\mathcal{L}_{e^+e^-}$ is not necessarily equal to $\mathcal{L}_{e^-e^-}$.

Assuming that the mean number of Compton interactions of an electron in a laser pulse (the Compton-conversion probability) is 1, the *conversion coefficient* $k \equiv n_\gamma/n \approx 1 - \mathrm{e}^{-1} = 0.63$, where n_γ is the number of scattered photons. The luminosity of a $\gamma\gamma$ collider is approximately

$$\mathcal{L}_{\gamma\gamma} = (n_\gamma/n)^2\,\mathcal{L}_{ee} \approx (0.63)^2\,\mathcal{L}_{ee}$$

However, if beams with smallest possible emittances and stronger beam focusing in the horizontal plane are used, $\mathcal{L}_{\gamma\gamma}$ can, in principle, be made higher than $\mathcal{L}_{e^+e^-}$ (see Section 3).

In the conversion region, a photon of energy ω_0 is scattered on an electron with energy E_0 at a small collision angle α_0 (see Figs. 1 and 2). The energy of the scattered photon ω depends on its angle ϑ relative to the motion of the incident electron as follows: [2]

$$\omega = \frac{\omega_m}{1 + (\vartheta/\vartheta_0)^2} \tag{1}$$

where

$$\omega_m = \frac{x}{x+1} E_0 , \qquad \vartheta_0 = \frac{m_e c^2}{E_0} \sqrt{x+1} \approx \frac{0.511\sqrt{x+1}}{E_0/\mathrm{TeV}}\ \mu\mathrm{rad} \tag{2}$$

and

$$x = \frac{4E_0\omega_0}{m_e^2 c^4} \cos^2(\alpha_0/2) \approx 15.3\left[\frac{E_0}{\mathrm{TeV}}\right]\left[\frac{\omega_0}{\mathrm{eV}}\right] \approx 19\left[\frac{E_0}{\mathrm{TeV}}\right]\left[\frac{\mu\mathrm{m}}{\lambda}\right] \tag{3}$$

The quantity $m_e c^2 \sqrt{x+1}$ is the total c.m. energy of the system comprising a laser photon and an incident electron, and ω_m is the maximum energy of the scattered photon.

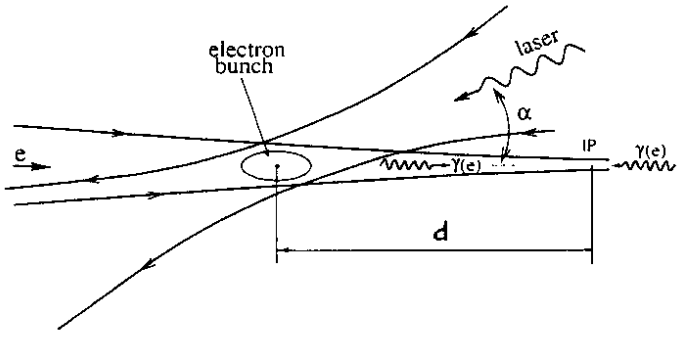

Fig. 1 The basic idea behind a photon collider.

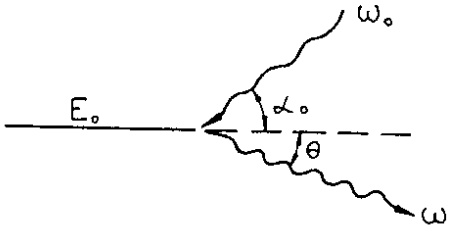

Fig. 2. Kinematics of Compton scattering.

[2] As an example from astrophysics, consider a photon of the 3-K cosmic background radiation colliding with a cosmic-ray proton of energy $E_p = 10^{20}$ eV ($\gamma \approx 10^{11}$). The incident photon's energy is $E_\gamma \approx 3\,\mathrm{kT} \approx 7\times10^{-4}$ eV and that of the scattered photon $\widetilde{E}_\gamma \approx 4\gamma^2 E_\gamma \approx 10^{19}$ eV. This spectacular gain in photon's energy comes at the expense of the proton, which loses a large fraction of its energy in a single collision. The Compton scattering on relic photons was considered soon after the discovery of cosmic background radiation [2].

The energy loss of cosmic-ray electrons in collisions with the thermal photons of starlight was first computed by Feenberg and Primakoff in 1948 [3]. They concluded that energetic electrons may undergo a sufficient number of Compton collisions in intergalactic space (travel time of about 10^9 years) to be removed from the cosmic radiation reaching the neighbourhood of the Earth. In terrestrial laboratories, the lifetime of a high-energy electron beam in an accelerator 'storage ring' is restricted due to Compton scattering on thermal radiation inside the beampipe [4].

The method of generating high-energy photons by Compton scattering of laser light on relativistic electrons [5], [6], which was proposed soon after the invention of the laser, has been used in several experiments [7]–[9].

According to (1), the photon scattering angle $\vartheta = \vartheta_0\sqrt{(\omega_m/\omega) - 1}$. For E_0 of a few hundred GeV, a typical photon scattering angle is a few μrad, with the lowest-energy photons scattered at the largest angles. The electrons scatter forward with an angle $\vartheta_e = \vartheta\, y(1-y)^{-1}$, where $y = \omega/E_0$.

The maximum energy of the scattered photon increases with ω_0. However, for $\omega_m\omega_0 > m_e^2c^4$, that is, $x > 2(1+\sqrt{2}) \approx 4.83$, the threshold is exceeded for the e^+e^- pair creation in the collision of a laser photon with a Compton-scattered gamma.[3] Since this process reduces the intensity of the high-energy photon beam, and could be a source of 'background events', the parameter x is restricted to values $x \leq 4.8$.

The wavelength of the laser photons corresponding to, say, $x = 4$ is

$$\lambda(x=4) \approx 5\,E_0[\mathrm{TeV}]\ \mu\mathrm{m} \tag{4}$$

which is comparable to that of the most powerful solid state lasers for $E_0 \lesssim 250$ GeV.

Both the energy spectrum and polarization of the backscatterd photons depend strongly on the polarizations of the incident electrons and laser photons. Colliding like-handed electrons and photons results in a flat distribution of backscatterd photons. If oppositely-handed electrons and photons are scattered, one obtains a peaked distribution of photons with energy up to about 80% of the incident electron beam energy (see Fig. 3, which is taken from [10]). This helicity configuration substantially improves the monochromaticity of the photon beam. Therefore, by polarizing the incident beams one can tailor the photon energy distribution to one's needs. The most useful region for experiments is that near the maximum photon energy.

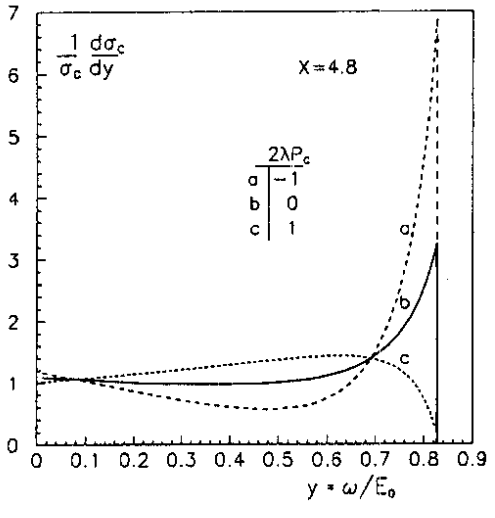

Figure 3: Spectrum of the Compton scattered photons for various polarizations of laser and electron beams.

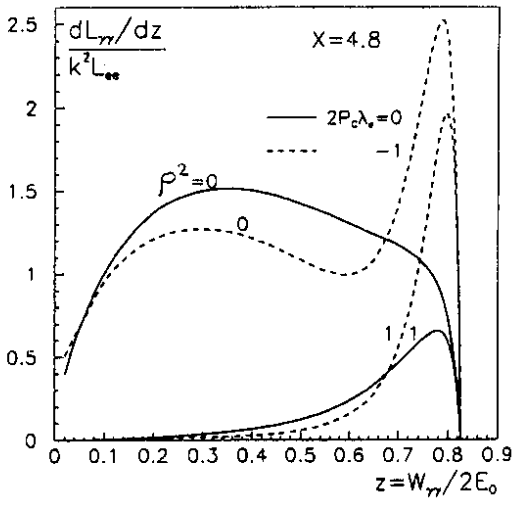

Figure 4: Spectral luminosity of $\gamma\gamma$ collisions for various polarizations and distances between conversion and interaction points.

The total Compton cross-section can be expressed as [10]

$$\sigma_c = \sigma_c^0(x) + 2\lambda_e P_c \sigma_c^1(x) \tag{5}$$

where λ_e is the mean electron helicity ($|\lambda_e| \leq 1/2$) and P_c is that of the laser photon ($|P_c| \leq 1$). In the region of our interest ($x = 1$ to 5), the total cross-section is hardly affected by the polarizations

[3] In an experiment at SLAC, a signal of 106 ± 14 positrons over background was observed in collisions of a 46.6-GeV electron beam with terawat pulses from a Nd:glass laser at 527 nm wavelength [9]. The positrons are thought to arise from a two-step process in which laser photons are backscattered to GeV energies by the electron beam, followed by a collision between the high-energy gamma and several laser photons to produce an e^+e^- pair. This result is the first laboratory evidence for inelastic light-by-light scattering involving only real photons.

of the incident beams [10]. The cross-section for Compton backscattering is approximately the *Thomson cross-section* $\sigma_{\rm T} = (8\pi/3)\, r_e^2$, where $r_e = {\rm e}^2/(4\pi m_e c^2) = 2.82 \times 10^{-13}$ cm is the classical radius of the electron (i.e., the radius of a cloud of charge e with electrostatic potential energy that is equal to the electron rest-mass energy).

The Compton-scattered photons have an average helicity $\langle\lambda_\gamma\rangle \neq 0$ if either the laser light has a circular polarization $\rm P_c \neq 0$ or the incident electrons have a mean helicity $\langle\lambda_e\rangle \neq 0$. In the case $2{\rm P_c}\lambda_e = -1$, which results in a good monochromaticity of the backscattered photon beam, the average degree of circular polarization of the photons within the high-energy peak of the luminosity distribution amounts to (90 to 95)%. While the lasers naturally produce linearly polarized light, any combination of circular and linear polarization can be produced using quarter-wave plates.

In a collision of two photons, the possible helicities are 0 or 2. For example, the Higgs boson is produced in the $J_z = 0$ state, whereas the background processes $\gamma\gamma \to f\bar{f}$ are suppressed for this helicity configuration. The circular polarization of the photon beams is therefore an important asset, for it can be used both to enhance the signal and suppress the background.

3 Beam characteristics

Along with control over both the energy distribution and polarization of the photon beams, high luminosities will give a photon collider the potential for a very valuable physics program. Due to the absence of beam-beam effects at the interaction point, a machine operating as a $\gamma\gamma$ or $e\gamma$ collider can, in principle, have a higher luminosity than an e^+e^- or e^-e^- linac. In the $\gamma\gamma$ case, such a high luminosity can be attained by using low-emittance electron sources or by laser cooling of the electron beams after the damping ring [11].

The absence of beam-beam effects in $\gamma\gamma$ collisions means that it is not necessary to have very flat linac beams. The spectral luminosity of $\gamma\gamma$ collisions strongly depends on beam characteristics, but only through the parameter ρ, the ratio of the intrinsic transverse spread of the photon beam to that of the original electron beam:

$$\rho \equiv \frac{d\,\theta_0}{\sqrt{2}\,\sigma_e} \approx 3.6\sqrt{x+1}\left(\frac{d}{\rm cm}\right)\left(\frac{\rm E_0}{\rm TeV}\right)^{-1}\left(\frac{\sigma_e}{\rm nm}\right)^{-1} \tag{6}$$

where d is the distance between the Compton interaction point and the $\gamma\gamma$ collision point, and σ_e is the radius that a round Gaussian linac beam would have at the collision point in the absence of a laser beam. As ρ increases, the monochromaticity of the luminosity distribution improves (because the lowest-energy photons, which scatter at the largest angles, do not pass through the collision point), but the total luminosity decreases. This is shown in Fig. 4, which is taken from [10]. For unpolarized beams, the full width at half maximum is $\Delta\omega_{1/2} \approx \omega_m/(x+2)$.

If the Compton interaction point is too far from the $\gamma\gamma$ collision point, the angular spread of the backscattered photon beam, which is of the order of $1/\gamma$, will render the collision point too diffuse. On the other hand, the greater the distance between these two points, the more monochromatic the photon energy spectrum. For a typical photon collider, $d \lesssim 1$ cm.

At the Compton interaction point, the electron beam is about 100 times wider than it would be at the ee collision point in the absence of a laser beam. However, since the backscattered photons follow the direction of the incident electrons, they are automatically 'focused' to their collision point.

An e^-e^- linac is better suited for photon collisions than an e^+e^- collider because (a) the very small energy spread required of an e^+e^- machine is not needed for a photon collider, and (b) it is easier to produce polarized electrons than positrons. In both machines the polarization is easily reversible. Recent progress in electron source technology at KEK and SLAC has ensured that

highly-polarized e^- beams will be available at a photon collider, enabling one to fully exploit the physics potential of the machine.

4 Laser requirements

In order to attain maximum luminosity, every electron bunch in the accelerator should collide with a laser pulse of sufficient intensity for 63% of the electrons to undergo a Compton scattering. This requires a laser system with high average power, capable of producing pulses that would match the temporal spacing of electron bunches. The laser power is minimized when the Rayleigh range of the laser focus [4] and the laser pulse width are matched to the electron bunch length. For instance, the proposed JLC e^+e^- collider is designed to have trains of 85 100-micron bunches separated by 1.4 ns, with 120 trains per second. This means that $85 \times 120 = 10,200$ laser pulses with a duration of approximately 1 ps must be produced every second. [5] To avoid nonlinear electrodynamic effects, the maximum pulse energy should not exceed 1 joule. Therefore, the laser system ought to deliver 10 kW of average power in pulses of a terawatt peak power, matched to the JLC bunch structure.

These requirements could be satisfied, for instance, by modifying the *Mercury laser* developed at the Lawrence Livermore Lab (LLNL) for a laser fusion application, as proposed by Jeff Gronberg and his collaborators [12]. The *Mercury laser* is designed to generate pulses of 100 J with a width of (2 to 10) ns at a rate of 10 Hz. An initial low-energy picosecond pulse is 'chirped' to produce a nanosecond pulse. Once amplified in the *Mercury*, the pulse can be recombined back to the picosecond level as long as it has retained a Gaussian profile after amplification. The technique of chirped-pulse amplification, invented by D. Strickland and G. Mourou in 1985, is at the heart of all laser designs that can produce terawatt peak power [13], [14]. The *Mercury laser* will use Ytterbium-doped crystals (Yb:S-FAP), pumped by diode arrays, to deliver 100 J at 10 Hz with $\varepsilon = 10\%$ efficiency for converting wall plug power to laser light. The long upper state lifetime of the crystal ($\tau = 1.26$ ms) allows the laser to be pumped more slowly, reducing the required peak diode power:

$$\text{Diode power} = \frac{\mathrm{N_{bunch}} \times \mathrm{E_{pulse}}}{\varepsilon \times \tau} = \frac{85 \times 1\,\mathrm{J/pulse}}{0.1 \times 1.26\ \mathrm{ms}} \approx 0.7\ \mathrm{MW} \tag{7}$$

The wavelength of the photons emitted by the *Mercury laser* is 1.047 μm. According to (4), $\lambda(x = 4) \lesssim 0.5$ μm for $\mathrm{E_0} \lesssim 100$ GeV. At these energies, one could use nonlinear crystals to generate higher harmonics, rays possessing a multiple of the frequency of the incoming laser light. The nonlinear response of a crystal can give rise to exchange of energy between a number of electromagnetic fields of different frequencies. For instance, half of the energy of an optical wave of frequency ω_0 propagating through the crystal can be converted to that of a wave at $2\omega_0$ (the so-called *second harmonic*). The single 0.52-μm pulse of 50 J from the *Mercury laser* must then be subdivided into 50 1-J pulses separated by 1.4 ns through a system of beam splitters and optical

[4] In general, the beam emitted from a laser can be approximated by a perfect plane wave with an ideal Gaussian intensity profile. However, it is impossible to have a perfectly collimated laser beam because light waves, as they propagate, spread transversely due to diffraction. In most laser applications it is necessary to focus, modify or shape the laser beam using lenses and other optical devices. The plane at which a Gaussian beam is made flat is called a 'Gaussian waist'. The waist radius of a laser beam with wavelength λ is $w_0 = (Z_\mathrm{R}\lambda/\pi)^{1/2}$, where Z_R, the *Rayleigh range*, is the depth of focus of a focused Gaussian beam (the distance over which the beam radius spreads by a factor of $\sqrt{2}$). The beam area at the waist is therefore $A = {w_0}^2\,\pi = \lambda Z_\mathrm{R}$.

[5] To produce one backscattered photon per electron, the laser photons must cover the full transverse area of the laser pulse: $A = \mathrm{N}_\gamma\sigma_c$, where N_γ is the number of laser photons in the pulse and σ_c is the effective cross-section per photon. Because of diffraction, $A = \lambda\ell$, where ℓ is the effective length of the laser pulse ($\ell \approx$ Rayleigh range $\approx$ electron bunch length). Taking the pulse length to be 1 ps and the laser wavelength 1 μm, and using the value of the Compton cross-section given earlier, we find $\mathrm{N}_\gamma = \lambda\ell/\sigma_c \approx 10^{19}$. The pulse energy is therefore $\mathrm{E_{pulse}} = \mathrm{N}_\gamma\,\omega_0 \approx 2$ J.

delay lines. A set of twelve of these lasers, each running at 10 Hz, could then be combined to provide the required repetition rate of 120 Hz [12].

5 Physics in $\gamma\gamma$, $e\gamma$ and e^-e^- collisions

We can imagine the following three scenarios:

- New particles and/or interactions will be discovered at the Tevatron and LHC proton colliders. These new phenomena would be better understood if they are studied in different processes. For instance, $\gamma\gamma$, $e\gamma$ and e^-e^- interactions can provide sensitive probes into the physics of supersymmetry, and may even exceed the mass reach of an e^+e^- machine;

- The two proton colliders will discover and study the Higgs boson, but no signatures of new physics will be observed. In this case a thorough exploration of the Higgs sector of the Standard Model (SM) will be undertaken with e^+e^- and photon colliders. The rich set of final states in $\gamma\gamma$, $e\gamma$ and e^-e^- collisions will play an essential role in measuring the mass, two-photon width, spin and parity of the Higgs boson, which are difficult to determine with only one initial state.

- A photon collider is built *before* any new particles or interactions are discovered.

In what follows we shall assume that at the interaction point of a photon collider $\gamma\gamma$, $e\gamma$ and e^-e^- collisions take place simultaneously with comparable luminosities, but at different centre-of-mass energies ($2\,\mathrm{E_0}$ for e^-e^-, $1.8\,\mathrm{E_0}$ for $e\gamma$ and $1.6\,\mathrm{E_0}$ for $\gamma\gamma$ collisions).

Higgs boson physics

To account for the observed mass spectrum of the field quanta, one postulates the existence of a *Higgs field*, which is a scalar under spatial rotations but is a weak isodoublet. The coupling of the Higgs field to the vector fields that mediate the electroweak interaction is arranged so as to give the W and Z masses in the 100 GeV range, while maintaining the photon mass at zero. The W- and Z-boson masses are fixed by the electroweak mixing angle θ_{W} (also called the Weinberg angle).

In the Standard Model, a theory with only one isodoublet of scalar bosons, the coupling of a fermion to the scalar Higgs field is proportional to the mass of the fermion. The Higgs boson mass, which is not fixed by the Weinberg angle, represents a free parameter of the model. Precision electroweak data suggest that the most likely mass for the SM Higgs boson is just above the limit of 114 GeV set by direct searches at LEP [15].

Ideally, one would like to determine, *in a model-independent way*, the mass, total width, spin, parity and CP properties of the Higgs boson, as well as its tree-level and one-loop induced couplings.

In $\gamma\gamma$ collisions, the Higgs boson with mass M_h will be produced as a sigle s-channel resonance: $\gamma\gamma \to h \to \bar{b}b$, WW, ZZ, $\tau\tau$, gg, $\gamma\gamma$ .... The reaction $\gamma\gamma \to h$ proceeds via a 'loop diagram', and receives contributions from all particles with mass and charge (see Fig. 5). The total width of the Higgs boson with $\mathrm{M}_h \lesssim 300$ GeV is much smaller than the characteristic width of the $\gamma\gamma$ luminosity spectra (see Fig. 9). The Higgs boson production rate is (see the Appendix)

$$\mathrm{N}_{\gamma\gamma\to h} = \frac{\mathrm{d}\mathrm{L}_{\gamma\gamma}}{\mathrm{d}W_{\gamma\gamma}} \frac{4\pi^2\,\Gamma(h\to\gamma\gamma)}{\mathrm{M}_h{}^2}\,(1+\lambda_1\lambda_2) \equiv \mathrm{L}_{\gamma\gamma}\,\sigma^{\mathrm{eff}}_{\gamma\gamma\to h} \tag{8}$$

In this expression we introduced the *effective cross-section* for $\gamma\gamma \to h$:

$$\sigma^{\mathrm{eff}}_{\gamma\gamma\to h} \equiv \frac{\mathrm{d}\mathrm{L}_{\gamma\gamma}}{\mathrm{d}W_{\gamma\gamma}} \frac{\mathrm{M}_h}{\mathrm{L}_{\gamma\gamma}} \frac{4\pi^2\,\Gamma(h\to\gamma\gamma)}{\mathrm{M}_h{}^3}\,(1+\lambda_1\lambda_2) \tag{9}$$

where $\Gamma(h \to \gamma\gamma)$ is the two-photon width of the Higgs boson, $W_{\gamma\gamma}$ is the $\gamma\gamma$ invariant mass, and λ_i are the photon helicities; $L_{\gamma\gamma}$ is defined as the $\gamma\gamma$ luminosity at the high-energy luminosity peak.

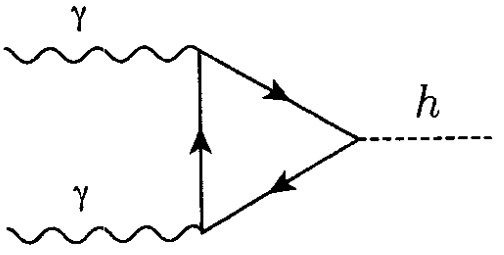

Fig. 5 The process $\gamma\gamma \to$ Higgs boson.

The effective cross-section for $(dL_{\gamma\gamma}/dW_{\gamma\gamma})(M_h/L_{\gamma\gamma}) = 7$ and $\lambda_1\lambda_2 = 1$ is shown in Fig. 6 [16]. We see that for M_h = (120 to 250) GeV the effective cross-section in $\gamma\gamma$ collisions is larger than that in e^+e^- annihilations by a factor of 6 to 30. About 10^4 light SM Higgs particles can be produced for a total $\gamma\gamma$ luminosity of 100 fb^{-1}.

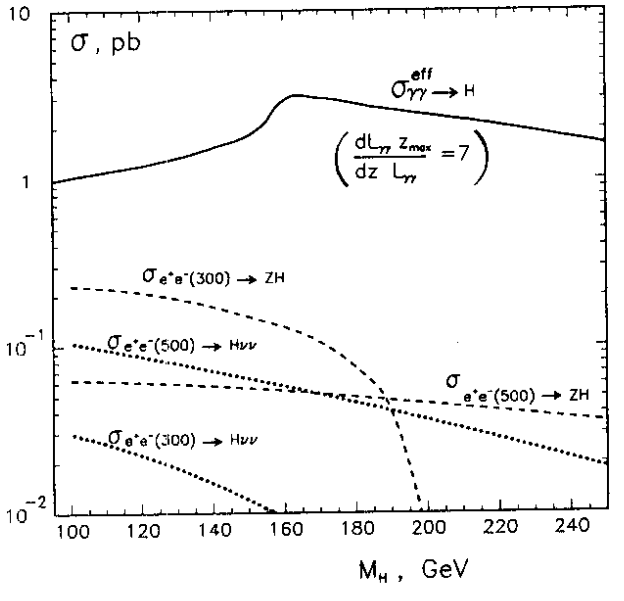

Fig. 6 Cross-sections for Higgs production in $\gamma\gamma$ and e^+e^- collisions.

At a photon collider, the Higgs boson can be detected either as a peak in the invariant mass distribution or by conducting an energy scan exploiting the sharp high-energy edge of the $\gamma\gamma$ luminosity distribution. The latter method should yield an accurate measurement of the Higgs mass [17]. Detailed Monte Carlo studies using detector simulations indicate that a Higgs signal can be observed well above the background, with the statistical error on the Higgs production cross-section at the (10 to 30)% level in the mass range M_h = (114 to 170) GeV [18], [19].

The number of $h \to X$ events, where $X = (\bar{b}b, \mathrm{WW}, \mathrm{ZZ})$, is given by (see the Appendix)

$$N_{h\to X} = \mathcal{L}\,\frac{4\pi^2\,\Gamma(h\to\gamma\gamma)\,B(h\to X)}{{M_h}^2}\,(1+\lambda_1\lambda_2) \tag{10}$$

Here $B(h \to X) \equiv \Gamma(h \to X)/\Gamma_h$ is the corresponding branching ratio (Γ_h is the total width) and

$$\mathcal{L} \equiv \left.\frac{dL_{\gamma\gamma}}{dW_{\gamma\gamma}}\right|_{M_h} \qquad \text{for} \quad J_z = 0 \tag{11}$$

Since the Higgs boson has spin zero, the colliding photons must be in an $J_z = 0$ state.

The dominant decays of a Higgs boson with a mass below the W^+W^- threshold are into fermion-antifermion pairs. In the Born approximation, the partial width to any fermion channel is

$$\Gamma(h \to \bar{f}f) = N_c \frac{G_F m_f^2}{4\pi\sqrt{2}} M_h \beta_f^3 \tag{12}$$

where N_c is 1 for leptons and 3 for quarks, m_f is the fermion mass, $G_F \approx 1.16 \times 10^{-5}$ GeV^{-2} is the Fermi constant, and $\beta_f \equiv (1 - 4m_f^2/M_h^2)^{1/2}$ is the velocity of the final-state fermions.

A Higgs boson with mass $M_h \lesssim 140$ GeV decays predominantly to $\bar{b}b$. The main background to $\gamma\gamma \to h \to \bar{b}b$ is the continuum production of $\bar{b}b$ and $\bar{c}c$ pairs. Another potentially serious background is due to heavy quark pair production accompanied by the radiation of an additional gluon. Although these backgrounds are quite large, they can be very effectively suppressed by exploiting the polarization dependence of their cross-sections and by the use of angular and kinematical cuts. The results of a Monte Carlo simulation of $\gamma\gamma \to h \to \bar{b}b$ for $M_h = 120$ GeV is shown in Fig. 7 [20].

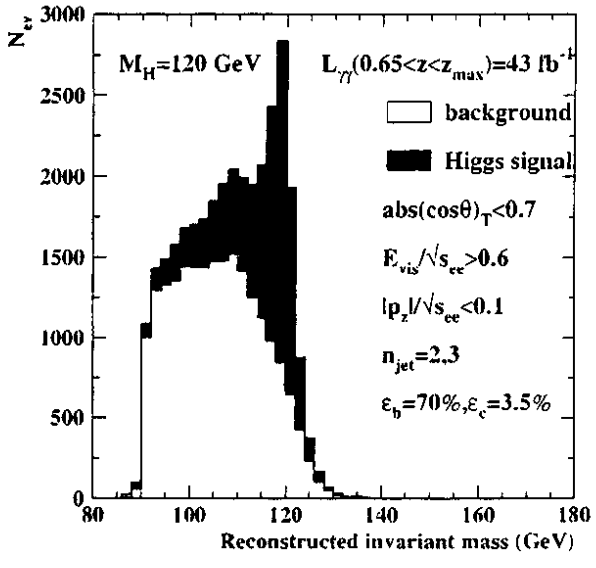

Fig. 7 Mass distribution for Higgs signal and heavy quark background.

The Higgs boson can also decay into gauge boson pairs. The $\bar{f}f$, WW and ZZ decays are the only two-body decay modes of h that occur at tree level. At one-loop, the decays $h \to gg$, $\gamma\gamma$, γZ are possible. The decay widths of the Higgs boson to physical W^+W^- or ZZ pairs are given by

$$\Gamma(h \to \mathrm{WW,\ ZZ}) = \delta_V \frac{G_F M_h^3}{16\pi\sqrt{2}} \left(1 - x_V + 3x_V^2/4\right) \beta_V \tag{13}$$

where $x_V = 4M_V^2/M_h^2$ and $\delta_V = 2$ or 1 for V = W or Z, respectively. Summed over $W^\pm$ and Z,

$$\Gamma(h \to \mathrm{VV}) \approx \frac{M_h^3}{2} \text{ [TeV units]} \tag{14}$$

Below the W^+W^- and ZZ thresholds, the Higgs boson can decay into vector boson pairs VV* (V = $W^\pm$, Z), with one of the gauge bosons off-shell. These decay modes can be significant, especially as M_h approaches the real WW and ZZ thresholds. The corresponding widths, summed over all channels available to the W* or Z*, are given in [21].

The SM Higgs boson with M_h = (140 to 190) GeV is expected to decay predominantly into WW* (below the WW threshold at $2M_W$) and WW pairs. In this energy region the large continuum background of W pairs is not easily suppressed. However, this decay mode should permit the detection of a Higgs signal below and slightly above the threshold for WW pair production [22].

The Feynman diagrams contributing to $h \to \gamma\gamma$ for spin-1/2, spin-1 and spin-0 loops are shown in Fig. 8. The width is given by [21]

$$\Gamma(h \to \gamma\gamma) = \frac{\alpha^2 G_F}{128\pi^3\sqrt{2}} M_h^3 \left| \sum_{i=1}^{n} N_{ci} Q_i^2 \mathcal{F}_i \right|^2 \tag{15}$$

where N_{ci} is the color multiplicity of particle i (3 for quarks and 1 otherwise) and Q_i is the electric charge in units of e; the functions $\mathcal{F}_i$ are given in [21]. The $h \to \gamma\gamma$ decay mode evidently probes the existence of heavy charged particles. When the particle in the loop is much heavier than the Higgs boson, $\mathcal{F}_0 \to -1/3$, $\mathcal{F}_{1/2} \to -4/3$ and $\mathcal{F}_1 \to 7$. Note the opposite sign between fermion and W loops.

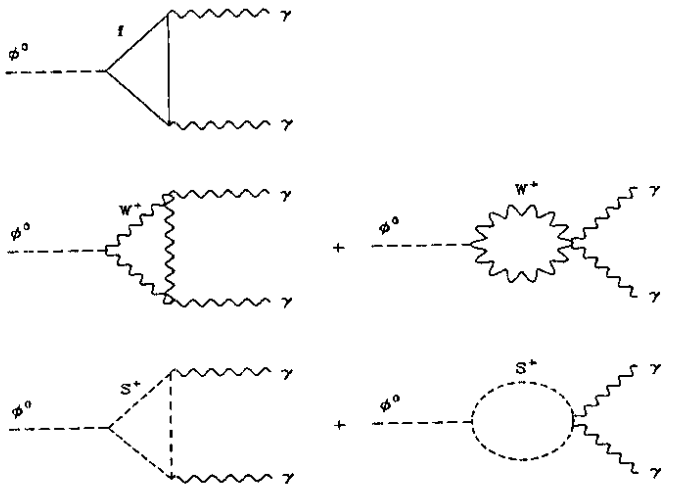

Fig. 8 Diagrams contributing to $h \to \gamma\gamma$.

The total Higgs boson decay width in the Standard model is shown in Fig. 9 [23]. Below $M_h \approx 140$ GeV, the Higgs boson is quite narrow with $\Gamma_h < 10$ MeV. As the WW* and ZZ* channels become accessible, the width increases rapidly, reaching a value of about 1 GeV at $M_h \approx 200$ GeV.

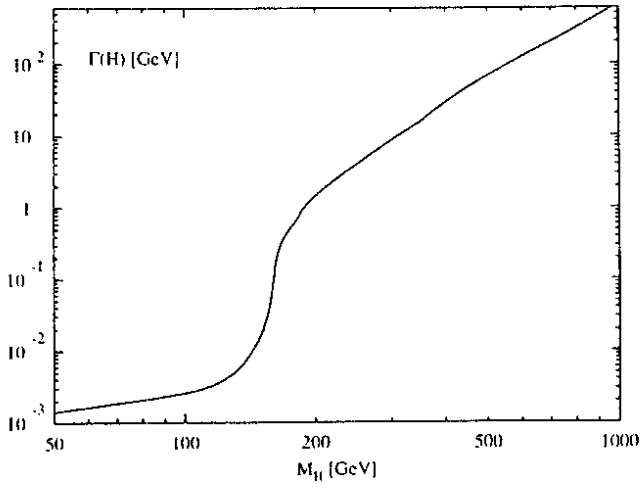

Fig. 9 Total Higgs-boson decay width in the Standard Model.

The total width Γ_h is of special interest because its value can be used to compute individual partial widths. The latter provide the most direct probe into the nature of the Higgs particle. Any deviation of a partial width from the SM prediction can be directly compared with the prediction of an alternative theoretical model, such as the minimal supersymmetric model (MSSM).

The fractional error on $\Gamma(h \to \gamma\gamma)\mathrm{B}(h \to \bar{b}b$ or WW, ZZ) for an integrated luminosity of 50 fb^{-1} is illustrated in Fig. 10 [18]. A more recent Monte Carlo simulation of $\gamma\gamma \to h \to \bar{b}b$ has shown that the two-photon width of a Higgs boson with mass $M_h = 120$ GeV can be measured with a statistical accuracy of about 2% for an integrated luminosity in the high-energy peak of 40 fb^{-1} [20]. As a result, the total decay width of the Higgs boson can be determined in a model-independent way with a precision of about 12%, as we shall now explain.

Assuming that the branching ratio $\mathrm{B}(h \to \bar{b}b)$ can be measured to an accuracy of about 1% in the process $e^+e^- \to Zh$ [24], the two-photon width $\Gamma(h \to \gamma\gamma)$ can be calculated to a precision of about 2% [25] using

$$\Gamma(h \to \gamma\gamma) = \frac{\{\Gamma(h \to \gamma\gamma)\,\mathrm{B}(h \to \bar{b}b)\}}{\{\mathrm{B}h \to \bar{b}b)\}} \tag{16}$$

This level of accuracy is sufficient to observe contributions of additional heavy states to the 'loop diagram'.

If we further assume that the branching ratio $\mathrm{B}(h \to \gamma\gamma)$ can be measured in e^+e^- collisions with a precision of (10 to 15)% [26], then the total width of the Higgs boson

$$\Gamma_h \equiv \frac{\{\Gamma(h \to \gamma\gamma)\,\mathrm{B}(h \to \bar{b}b)\}}{\{\mathrm{B}(h \to \gamma\gamma)\}\{\mathrm{B}(h \to \bar{b}b)\}} \tag{17}$$

can be determined in a *model-independent* way to an accuracy limited by the measurement error on $\mathrm{B}(h \to \gamma\gamma)$ [25].

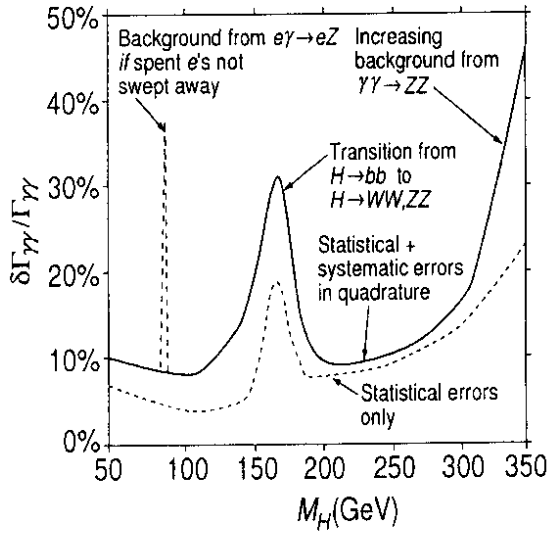

Fig. 10 Fractional error on $\Gamma(h \to \gamma\gamma)\mathrm{B}(h \to \bar{b}b$ or WW, ZZ).

The CP properties of any neutral Higgs boson that may be produced at a photon collider can be explored by controlling the polarizations of Compton-scattered photons [27]. A CP-even Higgs boson couples to the combination $\boldsymbol{\varepsilon}_1 \cdot \boldsymbol{\varepsilon}_2$, while a CP-odd Higgs boson couples to $(\boldsymbol{\varepsilon}_1 \times \boldsymbol{\varepsilon}_2) \cdot \boldsymbol{k}_\gamma$, where $\boldsymbol{\varepsilon}_i$ are photon polarization vectors. The scalar (pseudoscalar) Higgs boson couples to linearly polarized photons with a maximal strength if the polarization vectors are parallel (perpendicular):

$$\sigma \propto 1 \pm l_1 l_2 \cos 2\phi \tag{18}$$

where l_i are the degrees of linear polarization and ϕ is the angle between l_1 and l_2. The signs $\pm$ correspond to the CP $= \pm 1$ scalar particles.

Charged pair production

In lowest order, the main contribution to the two-photon production of charged pairs comes from the Feynman diagram in Fig. 11.[6] The production of charged particle pairs in e^+e^- collisions proceeds through (a) s-channel (annihilation) diagrams with virtual γ and Z, and (b) t-channel exchange reactions where new particles can contribute. The s-channel processes mediated by the Z-boson depend on the weak isospin of the final-state particles. In contrast, the couplings of the final-state particles in $\gamma\gamma$ collisions can be determined unambiguously. Combined measurements of pair production in e^+e^- and $\gamma\gamma$ collisions can therefore be used to disentangle various couplings of the charged Higgs bosons.[7]

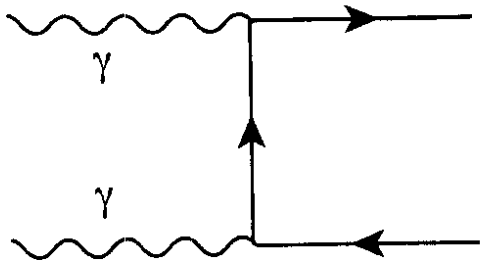

Fig. 11 Diagram describing $\gamma\gamma \rightarrow$ charged pair.

The cross-sections for production of pairs of scalar particles (S), fermions (F) and W-bosons (W) in unpolarized $\gamma\gamma$ and e^+e^- collisions, shown in Fig. 12, are of the form [10]

$$\sigma = \frac{\pi\alpha^2}{\mathrm{M}^2} f(x) \tag{19}$$

where M is the particle mass and $x = W^2/4\mathrm{M}^2$ (W is the invariant mass, i.e., the centre-of-mass energy of the colliding beams). We see that the production cross-sections in $\gamma\gamma$ interactions are larger than those in e^+e^- collisions by about an order of magnitude.

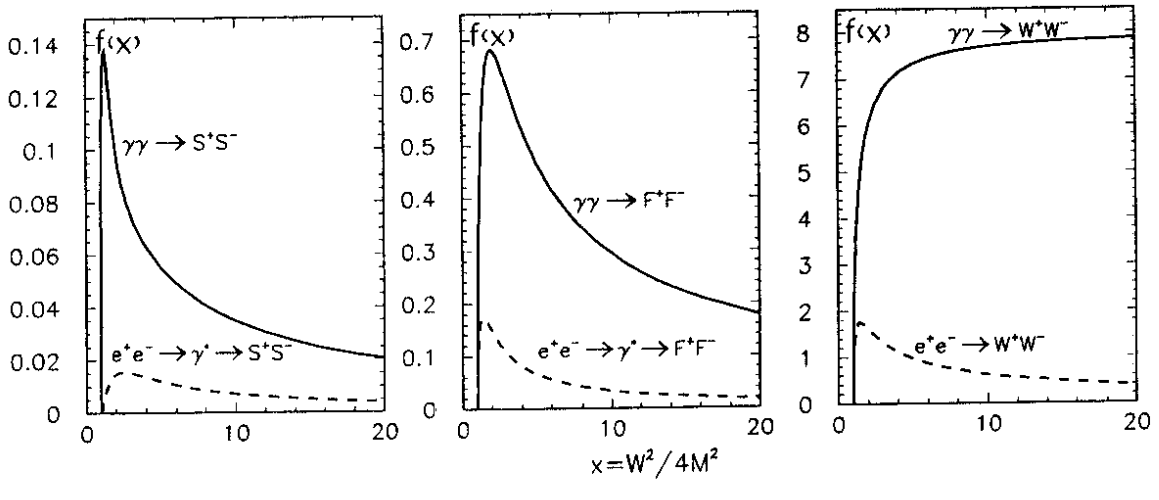

Fig. 12 Cross-sections for $\gamma\gamma$ or $e^+e^- \rightarrow$ charged pair.

[6] We do not show the four-line vertices generated by the boson self-interaction terms in the SU(2)×U(1) gauge-invariant Lagrangian density.

[7] At least five Higgs bosons are predicted in supersymmetric models: h^0, H^0, A^0, H^+ and H^-.

The total cross-section for $\gamma\gamma \to W^+W^-$ at centre-of-mass energies $\gtrsim 200$ GeV is about 80 pb. For an integrated $\gamma\gamma$ luminosity of 50 fb^{-1}, a few million W^+W^- pairs can be produced at a photon collider, comparable to the number of Z bosons detected at LEP. In contrast, each of the four LEP experiments collected only about 10^4 W-pair events.

Unlike the electrically neutral photon in quantum electrodynamics, the weak vector bosons carry 'weak charge'. Consequently, they can interact among themselves through the trilinear and quartic gauge boson vertices. Direct tests of the trilinear couplings are provided by e^+e^- and $p\bar{p}$ colliders through the processes $e^+e^- \to W^+W^-$, $Z\gamma$, ZZ and $p\bar{p} \to W^\pm\gamma$, W^+W^-, $W^\pm Z$, $Z\gamma$, ZZ. The signature for anomalous trilinear couplings is an excess of gauge boson pairs.

The LEP2 and Tevatron data have verified that the cross-sections for the production of weak gauge boson pairs agree with the Standard Model predictions, at least in the energy region close to the WW and ZZ production thresholds [28]. However, some estimates suggest that a much higher level of precision than the one attained so far is needed to test any anomalous gauge boson couplings [25]. While $e^+e^- \to W^+W^-$ involves potentially anomalous Z couplings, $\gamma\gamma \to W^+W^-$ isolates any non-standard photon couplings to the W boson. For the $J_z = 0$ state ($\lambda_1 = \lambda_2$), the Standard Model predicts that the W bosons are either longitudinal, or transverse with the same handedness. This property, coupled with the large cross-section (of the order of 10^2 pb), could be useful when looking for signals of new physics in the reaction $\gamma\gamma \to W^+W^-$ [29].

Physics in $e\gamma$ and e^-e^- collisions

The two main processes at a photon collider are $\gamma\gamma \to WW$ (see Fig. 11) and $e\gamma \to \nu W$ (see Fig. 13). Their total cross-sections at centre-of-mass energies $\gtrsim 200$ GeV are about 80 pb and 40 pb, respectively [30]. Both processes are sensitive to any anomalous photon couplings to the W boson. The missing momentum and angular dependence in $e\gamma \to \nu W$ are the best handles for distinguishing this reaction from the more frequent $\gamma\gamma \to WW$ process.

In an $e\gamma$ collision, a heavy charged particle can be produced concurrently with a light neutral one. If the mass difference between the final-state particles is large, the kinematical limit for the production of charged particles in $e\gamma$ collisions could be higher than that for the charged-pair production in e^+e^- interactions. An example is the production of the scalar electron and neutralino in the reaction $e\gamma \to \tilde{e}\tilde{\chi}_1^0$.

The key advantage of using e^-e^- beams is that they can be polarized to a high degree (about 90%). It has been shown that the Møller scattering $e^-e^- \to e^-e^-$ could yield a measurement of the Weinberg angle $\sin^2\theta_W$ to a precision of 10^{-4} [31]. Another interesting process is the t-channel reaction $e_L^-e_L^- \to W^+W^-$ with a heavy Majorana neutrino exchange. The corresponding cross-section is sizeable and has a characteristic s^2 energy dependence [32]. This process could reveal the existence of Majorana neutrinos with TeV masses.

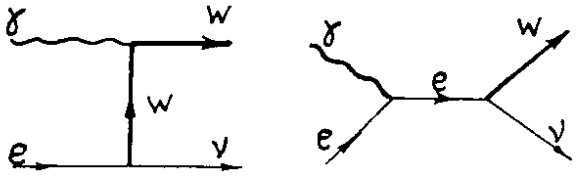

Fig. 13 Diagrams describing $e\gamma \to \nu W$

Appendix

For a $\gamma\gamma$ collider, the number of events of type X is given by

$$\mathrm{N_X} = \int \frac{\mathrm{dL}_{\gamma\gamma}}{\mathrm{d}W}\,\sigma_{\mathrm{X}}(W)\,\mathrm{d}W = \mathrm{L}_{\gamma\gamma}\int\left(\frac{1}{\mathrm{L}_{\gamma\gamma}}\frac{\mathrm{dL}_{\gamma\gamma}}{\mathrm{d}W}\right)\sigma_{\mathrm{X}}(W)\,\mathrm{d}W \tag{A.1}$$

where $\mathrm{L}_{\gamma\gamma}$ is the $\gamma\gamma$ luminosity and W the centre-of-mass energy of the colliding beams. We define the *effective cross-section* as

$$\sigma_{\mathrm{X}}^{\mathrm{eff}} \equiv \int\left(\frac{1}{\mathrm{L}_{\gamma\gamma}}\frac{\mathrm{dL}_{\gamma\gamma}}{\mathrm{d}W}\right)\sigma_{\mathrm{X}}(W)\,\mathrm{d}W \tag{A.2}$$

so that $\mathrm{N_X} = \mathrm{L}_{\gamma\gamma}\,\sigma_{\mathrm{X}}^{\mathrm{eff}}$.

A Higgs boson with mass $\mathrm{M}_h \lesssim 140$ GeV decays predominantly to $\bar{b}b$, and has a total width of only a few MeV (see Figs. 9 and 14 [23]). The main background to $\gamma\gamma \to h \to \bar{b}b$ is the continuum production of $\bar{b}b$ and $\bar{c}c$ pairs. Since the Higgs boson is such a narrow resonance, we may safely ignore interference effects between the pair-creation processes and the s-channel resonance production. In this case the $\gamma\gamma \to \bar{b}b$ cross-section decomposes into a sum of a $\bar{b}b$ continuum production cross-section and a Breit-Wigner contribution [33], [34]:

$$\sigma(\gamma\gamma \to \bar{b}b) = \sigma_c(\gamma\gamma \to \bar{b}b) + \sigma(\gamma\gamma \to h \to \bar{b}b) \tag{A.3}$$

where

$$\frac{\mathrm{d}\sigma_c(\gamma\gamma \to \bar{b}b)}{\mathrm{d}\cos\theta} = \frac{2\pi\alpha^2}{27\,W^2}\,\frac{1+\cos^2\theta}{1-\cos^2\theta}\,(1-\lambda_1\lambda_2) \qquad \text{for } \beta \to 1 \tag{A.4}$$

and

$$\sigma(\gamma\gamma \to h \to \bar{b}b) = \frac{8\pi\,\Gamma(h \to \gamma\gamma)\,\Gamma(h \to \bar{b}b)}{(W^2-\mathrm{M}^2)^2 + \Gamma_h^2\,\mathrm{M}^2}\,(1+\lambda_1\lambda_2) \tag{A.5}$$

In these expressions, $\beta = (1-4m_b^2/W^2)^{1/2}$, λ_i are the photon helicities, M is the Higgs boson mass, and Γ_h, $\Gamma(h \to X)$ are the total and partial decay widths, respectively.

Since $\Gamma_h \ll \mathrm{M}$, we can write

$$\frac{1}{\pi}\,\frac{\mathrm{M}\,\Gamma_h}{(W^2-\mathrm{M}^2)^2 + \Gamma_h^2\,\mathrm{M}^2} = \delta(W^2-\mathrm{M}^2) \tag{A.6}$$

This expression can be checked by setting $W^2 \equiv x$, $\mathrm{M}^2 \equiv a$ and integrating both sides over $\mathrm{d}x$. The number of $h \to \bar{b}b$ events is given by

$$\mathrm{N}_{h\to\bar{b}b} = \left.\frac{\mathrm{dL}_{\gamma\gamma}}{\mathrm{d}W_{\gamma\gamma}}\right|_{\mathrm{M}_h}\,\frac{4\pi^2\,\Gamma(h \to \gamma\gamma)\,\mathrm{B}(h \to \bar{b}b)}{\mathrm{M}_h{}^2}\,(1+\lambda_1\lambda_2) \tag{A.7}$$

where $\mathrm{B}(h \to X) \equiv \Gamma(h \to X)/\Gamma_h$ is the corresponding branching ratio. Since the Higgs boson has spin zero, the colliding photons must be in an $J_z = 0$ state.

We see that

$$\frac{\mathrm{d}\sigma_c(\gamma\gamma \to \bar{b}b)}{\mathrm{d}\cos\theta} \propto 1-\lambda_1\lambda_2\,, \qquad \sigma(\gamma\gamma \to h \to \bar{b}b) \propto 1+\lambda_1\lambda_2 \tag{A.8}$$

By arranging to collide highly polarized photon beams that have the same polarization, one can significantly reduce the background while enhancing the signal. A cut on $\cos\theta$ also improves the signal-to-background ratio, since the continuum $\bar{b}b$ pairs are preferentially produced at $|\cos\theta| \approx 1$, while the signal events are distributed uniformly in $\cos\theta$.

The luminosity spectra and the effective beam polarization in $\gamma\gamma$ collisions can be measured using the reaction $\gamma\gamma \to e^+e^-$ [35]. Luminosity measurements in $e\gamma$ collisions would rely on the Compton scattering process $e\gamma \to e\gamma$, which strongly depends on the circular polarization of the photon and the longitudinal polarization of the electron.

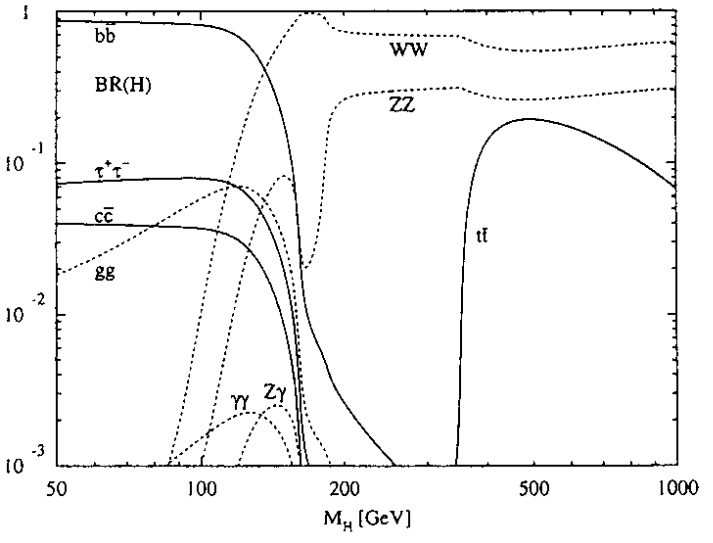

Fig. 14 Main branching ratios of the SM Higgs decay channels.

6 Proposal

We propose to build an X-band e^-e^- linac (based on the JLC/NLC design) and a terawatt laser system (based on the *Mercury* architecture) in order to produce Compton-scattered γ-ray beams for a photon collider. At the interaction point of the machine, $\gamma\gamma$, $e\gamma$ and e^-e^- collisions would take place simultaneously with comparable luminosities, but at different centre-of-mass energies. In $\gamma\gamma$ collisions, a light Higgs boson can be detected either as a peak in the invariant mass distribution or by conducting an energy scan exploiting the sharp high-energy edge of the $\gamma\gamma$ luminosity distribution. The latter method should yield an accurate measurement of the Higgs mass. Detailed Monte Carlo studies using detector simulations indicate that a Higgs signal can be observed well above the background. About 10^4 light SM Higgs particles can be produced for a total $\gamma\gamma$ luminosity of 100 fb^{-1}.

The initial $\gamma\gamma$ centre-of-mass energy would be 110 GeV, (corresponding to $2E_0 \approx 140$ GeV), which is just below the limit of 114 GeV set by direct Higgs boson searches at LEP. We envisage to gradually increase the centre-of-mass energy by adding rf cavities to the linac. Above the WW production threshold, a few million W^+W^- pairs can be produced for an integrated $\gamma\gamma$ luminosity of 100 fb^{-1}. This is comparable to the number of Z^0 bosons detected at LEP.

Once the $\gamma\gamma$ centre-of-mass energy has reached 200 GeV (corresponding to $2E_0 \approx 250$ GeV), a positron source would be added to the linac at a small additional cost, turning it into a high-luminosity e^+e^- collider. Such a machine could operate in a wide energy range, from the Z^0 peak to well above the ZZ threshold. The experience gained at the proposed facility could be exploited at a future linear collider (JLC/NLC, TESLA, CLIC).

Acknowledgements

I would like to thank Eri Asakawa, Keisuke Fujii, Kazuhisa Nakajima, Yasuhiro Okada, Valery Telnov and Kaoru Yokoya for helpful discussions. I am grateful to Bruce Yabsley for his interest and advice.

My interest in photon-photon scattering experiments was aroused in the late 1970s, while I was a graduate student, by a Paul Csonka's article published in 1967 [36]. The seminal work on photon colliders by Ilya Ginzburg, Gleb Kotkin, Valery Serbo and Valery Telnov in the early 1980s contributed greatly to the enthusiasm I have felt for this subject ever since. However, it was only after learning about the *Mercury* laser system from an article by Jeff Gronberg that I seriously considered the construction of such a machine.

References

[1] I. Ginzburg et al., Nucl. Inst. Meth. **205**, 47 (1983);
I. Ginzburg et al., *ibid* **219**, 5 (1984);
C. Akerlof, Preprint UMHE 81-59, Univ. of Michigan (1981).

[2] J. Felten, Phys. Rev. Lett. **15**, 1003 (1965)

[3] E. Feenberg and H. Primakoff, Phys. Rev. **73**, 449 (1948).

[4] V. Telnov, Nucl. Inst. Meth. **A260**, 304 (1987).

[5] F. Arutyunian and V. Tumanian, Phys. Lett. **4**, 176 (1963).

[6] R. Milburn, Phys. Rev. Lett. **10**, 75 (1963).

[7] O. Kulikov et al., Phys. Lett. **13**, 344 (1964).

[8] J. Ballam et al., Phys. Rev. Lett. **23**, 498 (1969).

[9] D. Burke et al., Phys. Rev. Lett. **79**, 1626 (1997).

[10] V. Telnov, Nucl. Inst. Meth. **A 355**, 3 (1995).

[11] V. Telnov, Nucl. Inst. Meth. **A 455**, 63 (2000).

[12] J. Gronberg et al., Proc. 2001 Part. Accel. Conf., Chicago.

[13] M. Perry and G. Mourou, Science **264**, 917 (1994).

[14] G. Mourou, C. Barty and M. Perry, Physics Today, January 1998, p. 22.

[15] B. Pietrzyk, Proc. 30^{th} Int. Conf. on High-Energy Phys., Osaka (2000).

[16] V. Telnov, Int. J. Mod. Phys. **A 13**, 2399 (1998).

[17] T. Ohgaki, Int. J. Mod. Phys. **A 15**, 2605 (2000).

[18] J. Gunion et al., UCD-97-5, hep-ph/9703330 (1997).

[19] G. Jikia and A. Tkabladze, Nucl. Inst. Meth. **A 355**, 81 (1995);
Phys. Rev. **D 54**, 2030 (1996).

[20] G. Jikia and S. Söldner-Rembold, Nucl. Inst. Meth. **A 472**, 133 (2001).

[21] J. Gunion et al., *The Higgs Hunter's Guide*, Addison-Wesley (1990).

[22] I. Ginzburg and I. Ivanov, Phys. Lett. **B 408**, 325 (1997).

[23] A. Djouadi et al., Comput. Phys. Commun. **108**, 56 (1998).

[24] M. Battaglia, hep-ph/9910271 (1999).

[25] E. Boos et al., Nucl. Inst. Meth. **A 472**, 100 (2001).

[26] E. Boos et al., DESY-2000-162, hep-ph/0011366 (2000).

[27] B. Grzadkowski and J. Gunion, Phys. Lett. **B 294**, 361 (1992).

[28] G. Bella et al., LEPEWWG/TGC/2000-01 (2000);
B. Abbot et al., Phys. Rev. **D 60**, 072002 (1999).

[29] M. Baillargeon, G. Belanger and F. Boudjema, Nucl. Phys. **B 500**, 224 (1997).

[30] I. Ginzburg et al., Nucl. Phys. **B 228**, 285 (1983).

[31] A. Czarnecki and W. Marciano, Int. J. Mod. Phys. **A 13**, 2235 (1998).

[32] C. Heush and P. Minkowski, Nucl. Phys. **B 416**, 3 (1994);
Phys. Lett. **B 374**, 116 (1996).

[33] D. Borden, D. Bauer and D. Caldwell, Phys. Rev. **D 48**, 4018 (1993).

[34] T. Barklow, SLAC-PUB-5364 (1990).

[35] Y. Yasui et al., Nucl. Inst. Meth. **A 335**, 385 (1993).

[36] P. Csonka, CERN yellow report TH 772 (1967); Phys. Lett. **B 24**, 625 (1967).